J Solution Chem (2007) 36:327–344
DOI 10.1007/s10953-006-9117-y

ORIGINAL PAPER

Ammonia Catalyzed Hydrolysis-Condensation Kinetics of Tetraethoxysilane/Dimethyldiethoxysilane Mixtures Studied by ^{29}Si NMR and SAXS

Yao Xu · Xianyong Sun · Dong Wu · Yuhan Sun · Yongxia Yang · Hanzhen Yuan · Feng Deng · Zhonghua Wu

Received: 8 June 2006 / Accepted: 30 August 2006 /
Published online: 6 February 2007

Abstract *In-situ* ^{29}Si liquid-state nuclear magnetic resonance (NMR) was used to investigate the ammonia catalyzed hydrolysis and condensation of the mixed systems of tetraethoxysilane (TEOS) and dimethyldiethoxysilane (DDS) dissolved in methanol. With ammonia catalysis, the hydrolysis reaction orders for TEOS and DDS in the mixed systems remained first order, which is similar to that observed for their corresponding single silane component precursor systems. The hydrolysis rate constant for TEOS in the mixed systems was larger than that of TEOS in the single silane component precursor systems. Meanwhile, the hydrolysis rate constants of DDS in the mixed precursor systems were smaller than those of DDS in the single silane component precursor systems. The hydrolysis and condensation kinetics showed more compatible hydrolysis-condensation relative rates between TEOS and DDS, which remarkably affected the final microstructure of the resulting silica particles. Small angle X-ray scattering (SAXS) experiments showed a typical double fractal structure in the particulate networks.

Keywords Reaction kinetics · ^{29}Si NMR · Hydrolysis · Condensation · Small angle X-ray scattering · Tetraethoxysilane (TEOS) · Dimethyldiethoxysilane (DDS)

Y. Xu (✉)· X. Sun · D. Wu · Y. Sun
State Key Laboratory of Coal Conversion, Institute of Coal Chemistry, Chinese Academy of Sciences, Taiyuan 030001, China
e-mail: xuyao@sxicc.ac.cn

Y. Yang· H. Yuan · F. Deng
State Key Laboratory of Magnetic Resonance & Atomic & Molecular Physics, Wuhan Institute of Physics and Mathematics, Chinese Academy of Sciences, Wuhan 430071, China

Z. Wu
Laboratory of Synchrotron Radiation, Institute of High Energy Physics, Chinese Academy of Sciences, Beijing 100039, China

1 Introduction

The sol-gel process has proven to be a highly effective method for the synthesis of glasses, ceramics, nanocrystallines and nanoscaled amorphous materials under mild conditions [1–5]. By introducing organic groups or polymers into the inorganic silica matrices, the properties of the sol-gel derived materials can be tailored at the molecular level according to different requirements [6, 7]. So far, a large number of SiO_2-based sol-gel derived hybrid materials have been prepared and are expected to be applied in optical devices [8], functional thin films [9] and membranes for gas separation [10]. Although a wealth of sol-gel synthetic approaches have been reported, a detailed understanding of the underlying reactive kinetics in the sol-gel process currently is not fully developed. Even for a single precursor, TEOS for example, athough the kinetics of the sol-gel reactions has been formulated at various levels of sophistication [1, 2, 11–14], the reactive pathway is not fully understood. Besides, no general rule can be used to guide the control of the sol-gel process [15, 16].

Reaction kinetics are highly sensitive not only to the nature of the starting precursor, but also to the pH and the solvent polarity of the reaction medium [1, 2, 17]. When TEOS, a commonly used inorganic precursor, is co-hydrolyzed together with an organic-substituted ethoxysilane monomer ($R_xSi(OEt)_{1-x}$, where R can be methyl, ethyl, phenyl, vinyl, 3-aminopropyl, 3-methacryloxypropyl or 3-glycidoxypropyl), many other factors add to the complexity of the initial reaction kinetics and the subsequent sol-gel process [18–20]. Therefore, an investigation on the reaction kinetics of TEOS and an organic-substituted monomer in a mixed precursor system becomes crucial for understanding the nature of the hybrid sol-gel process.

In double-precursor systems, the time sequence between hydrolysis, self-condensation and cross-condensation is highly complex and depends on the special reaction conditions, *e.g.*, the pH of the initial solution and the nature and number of substituents on the $R_xSi(OEt)_{4-x}$ molecule [21–25]. Some studies [22, 23, 25] have been reported that involved the time sequence of hydrolysis, self-condensation and cross-condensation using different double-precursor systems, but the results differ largely with different organic substitution on the precursor. Among the limited reports on the sol-gel kinetics of double-precursor systems, most were performed under acidic condition. Under acidic condition, hydrolysis is usually by far faster than condensation, so that oligomers of the hydrolyzed precursor can exist in solution and can be easily be detected by several experimental methods. Although the reverse occurs under basic conditions [1, 26], fewer studies have been made because they involve more difficult experiments. In the very few reports on base-catalyzed hydrolysis [27–29], studying the hydrolysis kinetics was not the main object of the research. In fact, the condensation species are not easy to observe because condensation is faster than hydrolysis under basic conditions and the condensed species can hardly be detected even by *in-situ* ^{29}Si NMR.

Riegel *et al*. [20] studied the ammonia-catalyzed hydrolysis and condensation of TMOS and RTMS (R = methyl, ethyl, propyl, vinyl or phenyl) by Raman spectroscopy. The main difficulty they encountered was that no intermediate hydrolysis species or condensation species were observed and Raman spectroscopy did not yield detailed quantitative data. Therefore, the kinetic rate constants could not be calculated. Despite the difficulties of the experiments, understanding the base-catalyzed sol-gel process with double-precursor systems is still necessary and important to produce proper organic-modified silica nanoparticles whose microstructures and performances will be different from those obtained *via* the acid-catalyzed route. Their wide usage will require further investigations to elucidate the early stages of the base-catalyzed sol-gel process. In the present work, the ammonia-catalyzed

Table 1 Reaction component compositions

Sample	Molar ratio of TEOS/DDS/H_2O/NH_3
(a)	0.61/0.61/1.8[a]/0.152
(b)	0.61/0.60/1.8[a]/0.243
(c)	0.61/0.61/1.8[a]/0.486
(d)	0.61/0.61/3.6[b]/0.152
(e)	0.61/0.61/5.4[c]/0.152
(f)	0.61/0.31/1.5[a]/0.152
(g)	0.61/0.15/1.35[a]/0.152

[a] $M_{H_2O} = 2M_T + M_D$.
[b] $M_{H_2O} = 4M_T + 2M_D$.
[c] $M_{H_2O} = 6M_T + 3M_D$. Here M_{H_2O}, M_T and M_D are the molar concentrations of H_2O, TEOS and DDS, respectively.

hydrolysis kinetics of TEOS/DDS mixtures in methanol are investigated and the detailed rate constants are determined.

2 Experimental

2.1 Materials and components

Reagent grade aqueous ammonium hydroxide (26% NH_3), anhydrous methanol, deionized water, TEOS (Acros, 99% purity) and DDS (TCI, 98% purity) were used as received. The reaction component compositions are presented in Table 1. Solutions (a) through (e) were prepared by the ammonia-catalyzed hydrolysis of an equimolar mixture of TEOS and DDS, which was held constant at 0.61 mol·m^{-3}. The effect of the ammonia concentration on the reaction rates can be derived by comparing the results for mixtures (a), (b) and (c). The effect of the water concentration on the reaction rates can be derived by comparing the results for mixtures (a), (d) and (e). The effect of the DDS/TEOS ratio can be derived from comparing the results for the mixtures (a), (f) and (g).

2.2 *In-situ* liquid-state ^{29}Si NMR experiments

In-situ liquid-state ^{29}Si NMR samples were prepared by mixing two solutions, A and B, at the temperature of 25 °C. Solution A, TEOS and DDS, was dissolved in half of the total methanol and stirred for 20 min. Solution B, deionized water and ammonia hydroxide, was dissolved in the other half of the methanol and was stirred for 5 min. The reaction was initiated by mixing solutions A and B. After 5 min of stirring, the sample was transferred to a NMR sample tube (5 mm O.D.) and analyzed immediately. Chromium(III) acetylacetonate, $Cr(acac)_3$ (1 wt.%), was added as the spin relaxation agent. Many studies [11, 30] have proven that $Cr(acac)_3$ has little effect on the reaction rate or the final product distribution. All *in-situ* liquid-state ^{29}Si NMR experiments were carried out in duplicate using a UNITY INOVA-500 Spectroscopy instrument. To achieve sufficient signal intensity, 168 scans were acquired for each spectrum with a 3 s pulse delay using a 90° pulse angle. The spectral frequency of ^{29}Si was 99.351 MHz. The resulting spectra were internally referenced to a tetramethylsilane (TMS) standard. The resonance peaks of the observed species were well resolved and could be integrated quantitatively. During the experiments, gelation did not occur and transesterification was negligible [11]. All these NMR experiments were conducted at 25 °C and the temperature was controlled to within ±0.1 °C.

As reference experiments, the individual hydrolysis of a single precursor, TEOS or DDS, were carried out under the same reaction conditions as mentioned above. The hydrolysis

and condensation rate constants were also calculated for comparison with those of mixed systems.

2.3 Interface characterization of the sols

According to the synthesis parameters detailed in Table 1, the sols were prepared and then subjected to Transmission Electron Microscopy (TEM, H600, Hitachi) and SAXS measurements. The SAXS experiments were performed on the 4B9A beam line at the Beijing Synchrotron Radiation Facility with a long-slit collimation system. The incident X-ray wavelength was 0.154 nm. The scattering angle 2θ was approximately 0 to 3°. The fractal structures of the organo-modified SiO_2 clusters were calculated.

2.4 Microstructure analysis of the xerogels

Solid-state ^{29}Si MAS NMR (MSL-400, Bruker) spectroscopy and X-ray photoelectron spectroscopy (XPS, PHI5300X, Perkin-Elmer) were also used to estimate the cross-condensation properties of the TEOS/DDS hybrid gel. The wet gels were obtained by freely gelating the sols used in the liquid-state ^{29}Si NMR experiments. The xerogels were obtained by drying the wet gels in air at room temperature and no further treatment was made. All of the ^{29}Si NMR experiments were performed on a Varian Infinityplus-400 spectrometer using a 7.5 mm probe under magic-angle spinning conditions. The resonance frequency was 79.5 MHz. The 90° pulse width was measured to be 4.8 μs. A repetition delay time of 100 s was used for the ^{29}Si single-pulse experiments.

3 Results

3.1 ^{29}Si NMR spectra and the concentrations of soluble Si species

In order to assign the ^{29}Si NMR chemical shifts to the different silicon species, the traditional notation was adopted [1]: thus D represents di-functional silicon in DDS, and Q represents tetra-functional silicon in TEOS. Then, the symbols D_m^n and Q_m^n denote the products of hydrolysis or condensation of DDS and TEOS, respectively, where m and n, respectively, are the number of siloxane bridges and the number of silanols surrounding the Si atom.

Figure 1a shows a typical, time-dependent, ^{29}Si NMR spectra obtained during the reaction of the mixed precursors. Figure 1b and c show the time-dependent ^{29}Si NMR spectra of the single precursor DDS system and the single precursor TEOS system, respectively. The chemical shifts of the soluble Si species shown in Fig. 1 are listed in Table 2. There were six peaks detected in the experiments. The two resonance signals at −0.36 ppm and −2.18 ppm correspond to D_0^1 and D_0^0, respectively, under basic condition [31]. The two resonance signals at −80.4 ppm and −81.3 ppm correspond to Q_0^1 and Q_0^0, respectively. These four signals were detected in every experiment. A weak resonance signal at 1.46 ppm belongs to D_0^2, but it does not appear in samples (d), (e), (f) or (g). A weak resonance signal at −78.3 ppm corresponds to Q_0^3. As can be seen from Fig. 1a, the hydrolysis of TEOS leads to the formation of Q_0^1 (mainly) and Q_0^3 (weak), but Q_0^2 was not observed. This last observation was probably due to the fast condensation of the intermediate species Q_0^2 under basic conditions, so that its signal intensity was below the detection limit of the liquid-state ^{29}Si-NMR spectrometer [11]. The biggest differences can be found among Fig. 1a–c and some signals corresponding

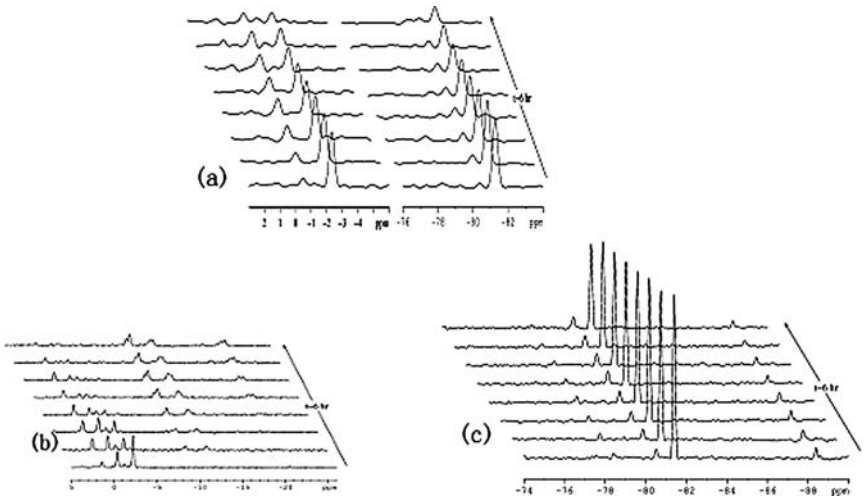

Fig. 1 Time-dependent liquid-state ^{29}Si NMR spectra of: (**a**) the TEOS/DDS systems with the molar ratio of TEOS/DDS/H_2O/NH_3 at 0.61/0.61/1.8/0.243; (**b**) the single precursor DDS system, and (**c**) the single precursor TEOS system

to dimers appeared in the spectra of the single precursor systems: D_1^0 at −9.45 ppm and D_1^1 at −8.92 ppm in Fig. 1b, Q_1^0 at −88.4 ppm in Fig. 1c, but not in Fig. 1a of the mixed precursor systems.

The relative concentrations of the intermediate soluble Si species were determined by integrating the resonance peak area at a fixed individual frequency in the NMR spectra. The integrated area of the initial Q_0^0 peak of TEOS (0.61 mol·dm^{-3}), observed without the presence of catalyst or water, was taken as being 100%. The disappearance of the monomers from their initial level and the appearance of one or more intermediate species are presented as functions of time in Fig. 2 for each studied reaction mixture. The time dependence of the monomer concentration (Q_0^0 or D_0^0) was obtained by fitting the experimental data with an exponential decay function of first order and the time-dependence curves shown for the intermediate species concentrations (Q_0^1 or D_0^1) are just to guide the eyes. The concentrations displayed in Fig. 2 are the basis for further calculations of the rate constants.

Comparing Fig. 2a–c, the extent of decrease of monomer concentration increases with increasing ammonia concentration. A similar trend can be seen by comparing Fig. 2a and d, but no obvious differences can be observed from comparing Fig. 2d with e. Increasing the concentration of DDS in the mixture speeds up the hydrolysis of the TEOS monomer

Table 2 Liquid-state ^{29}Si NMR chemical shift δ and the silicate structures

Species	Structures	δ(ppm)
D_0^2	$(Me)_2Si^*(OH)_2$	1.46
D_0^1	$(Me)_2Si^*(OEt)(OH)$	−0.36
D_0^0	$(Me)_2Si^*(OEt)_2$	−2.18
Q_0^3	$Si^*(OEt)(OH)_3$	−78.3
Q_0^1	$Si^*(OEt)_3(OH)$	−80.4
Q_0^0	$Si^*(OEt)_4$	−81.3

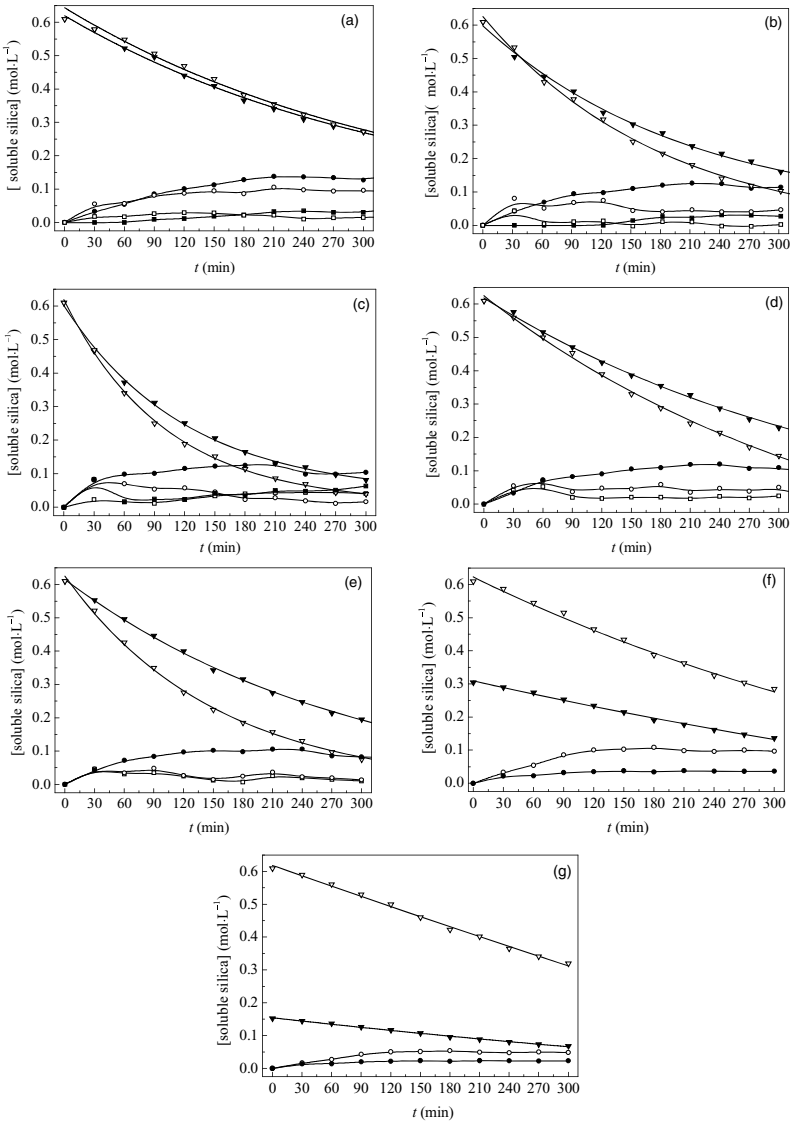

Fig. 2 Time-dependent soluble silicon species concentrations in the TEOS/DDS systems with molar ratios of TEOS/DDS/H_2O/NH_3 at: (**a**) 0.61/0.61/1.8/0.152; (**b**) 0.61/0.61/1.8/0.243; (**c**) 0.61/0.61/1.8/0.486; (**d**) 0.61/0.61/3.6/0.152; (**e**) 0.61/0.61/5.4/0.152; (**f**) 0.61/0.31/1.5/0.152; (**g**) 0.61/0.15/1.35/0.152, B▼ D_0^0, •D_0^1, ■D_0^2, ▽ Q_0^0, ○ Q_0^1, □Q_0^3

as seen by comparison of Fig. 2a, g and f, but no notable influence can be found on the hydrolysis rate of the DDS monomer itself. Therefore, a qualitative conclusion can be easily drawn from Fig. 2. That is, the hydrolysis of TEOS and DDS are both more sensitive to the ammonia concentration than to the water concentration, and the addition of DDS speeds up the hydrolysis of TEOS.

3.2 Hydrolysis kinetics

3.2.1 Hydrolysis-condensation mechanism and sol-gel kinetics model

Under basic conditions it is likely that water dissociates to produce nucleophilic hydroxyl anions in a rapid first step; the hydroxyl anion then attacks the silicon atom. Iler [32] and Keefer [33] proposed an S_N2–Si mechanism. Equation (1), in which OH^- displaces OR^- with inversion of the silicon tetrahedron, is as follows:

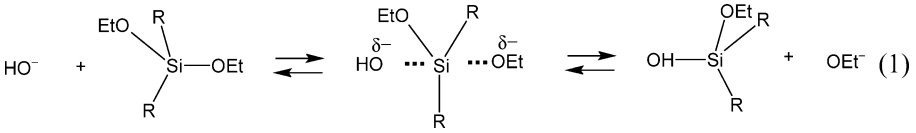

(1)

In Eq. (1), R = OEt for TEOS and R = CH_3 for DDS. This mechanism is affected by both steric and inductive factors; however, steric factors are more important because silicon acquires a little charge in the transition state. The most widely accepted mechanism for the condensation reaction involves the attack of a nucleophilic deprotonated silanol on a neutral silicate species, which was proposed by Iler [32] to explain condensation reactions in aqueous silicate systems. Pohl and Oserholtz [34] and Voronkov *et al*. [35] proposed essentially the same mechanism, Eqs. (2) and (3), to account for deuteroxide (hydroxyl) anion and general base-catalyzed condensation of silicon alkoxide.

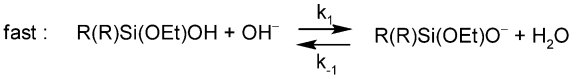

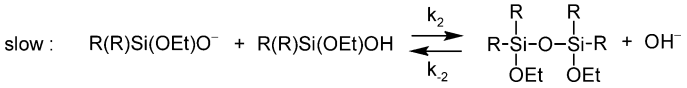

In above-mentioned rudimentary hydrolysis and condensation mechanism, how the various functional groups, (OR), (OH), and (OSi) are distributed on the silicon atoms is ignored. At this level, only three reactions and three rate constants are necessary to describe the functional group kinetics (Eqs. (4)–(6)), where *h* denotes hydrolysis, *cw* the condensation of water and *ca* the condensation of alcohol:

$$\mathrm{SiOR} + \mathrm{H_2O} \xrightarrow{k_h} \mathrm{SiO} + \mathrm{ROH} \tag{4}$$

$$2\mathrm{SiOH} \xrightarrow{k_{cw/2}} 2(\mathrm{SiO})\mathrm{Si} + \mathrm{H_2O} \tag{5}$$

$$\mathrm{SiOH} + \mathrm{SiOR} \xrightarrow{k_{ca/2}} 2(\mathrm{SiO})\mathrm{Si} + \mathrm{ROH} \tag{6}$$

In practice, hydrolysis and condensation occur concurrently, and at the nearest functional group level there are 15 distinguishable local chemical environments. Kay and Assink [36, 37] have represented the 15 silicate species in matrix forms. At this more sophisticated level, there are 165 distinguishable rate coefficients: $10k_h$, $55k_{cw}$ and $100k_{ca}$, considering only the forward reactions. If one goes further to the next-to-nearest functional group level, the

resulting number of rate constants will be huge. Thus, based on the above consideration, the precise sol-gel kinetics (including all of the determined rate constants) will be impossible to quantify experimental methods. Therefore, a simple sol-gel kinetic model proposed by Lee *et al*. [38] was adopted for the following kinetics calculations. This is a total model for hydrolysis and condensation kinetics, not a detailed rudimentary reaction model, so the obtained reaction orders must be fractional. These fractional reaction orders reflect the true complicated sol-gel process.

A simple sol-gel reaction kinetics model for TEOS is as follows:

$$Q_0^0 + \mathrm{H_2O} \xrightarrow{k_{\mathrm{Th1}}} Q_0^1 + \mathrm{ROH} \tag{7}$$

$$Q_0^1 + 2\mathrm{H_2O} \xrightarrow{k_{\mathrm{Th2}}} Q_0^3 + 2\mathrm{ROH} \tag{8}$$

$$Q_0^1 + Q_0^1 \xrightarrow{k_{\mathrm{Tc1}}} Q_1^0 + \mathrm{H_2O} \tag{9}$$

$$Q_0^3 + Q_0^3 \xrightarrow{k_{\mathrm{Tc2}}} Q_1^4 + \mathrm{H_2O} \tag{10}$$

As for DDS, the sol-gel reaction kinetics model is similar to that of TEOS and is as follows:

$$D_0^0 + \mathrm{H_2O} \xrightarrow{k_{\mathrm{Dh1}}} D_0^1 + \mathrm{ROH} \tag{11}$$

$$D_0^1 + \mathrm{H_2O} \xrightarrow{k_{\mathrm{Dh2}}} D_0^2 + \mathrm{ROH} \tag{12}$$

$$D_0^1 + D_0^1 \xrightarrow{k_{\mathrm{Dc1}}} D_1^0 + \mathrm{H_2O} \tag{13}$$

$$D_0^2 + D_0^2 \xrightarrow{k_{\mathrm{Dc2}}} D_1^2 + \mathrm{H_2O} \tag{14}$$

3.2.2 Hydrolysis kinetics of TEOS in TEOS/DDS mixtures

In reactions (7) to (10), all the reactive rates are dependent on $[NH_3]$ and $[H_2O]$, so the rate expression for the initial hydrolysis of TEOS is given by:

$$r_{\mathrm{T}} = -\frac{\mathrm{d}\left[Q_0^0\right]}{\mathrm{d}t} = k_{\mathrm{Th1}}\left[Q_0^0\right]^{\alpha}[\mathrm{NH_3}]^{\beta}[\mathrm{H_2O}]^{\gamma} \tag{15}$$

The exponents α, β and γ here are the reaction orders belonging to the TEOS monomer, NH_3 and H_2O, respectively. Because NH_3 was used as a catalyst during the hydrolysis and condensation processes, its concentration remained constant; the change of water concentration was less than 5% of the initial amount [38] so it was also regarded as being invariant when calculating reaction rate constants. If we define

$$k_{\mathrm{Th}}^1 = k_{\mathrm{Th1}}[\mathrm{NH_3}]^{\beta}[\mathrm{H_2O}]^{\gamma} \tag{16}$$

then the rate expression Eq. (15) can be simplified to

$$r_{\mathrm{T}} = -\frac{\mathrm{d}\left[Q_0^0\right]}{\mathrm{d}t} = k_{\mathrm{Th}}^1\left[Q_0^0\right]^{\alpha} \tag{17}$$

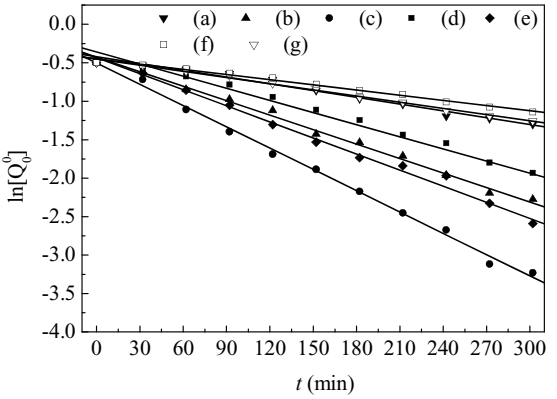

Fig. 3 Time-dependent TEOS monomer concentrations in the TEOS/DDS systems with the molar ratio of TEOS/DDS/H_2O/NH_3 at: (**a**) 0.61/0.61/1.8/0.152; (**b**) 0.61/0.61/1.8/0.243; (**c**) 0.61/0.61/1.8/0.486; (**d**) 0.61/0.61/3.6/0.152; (**e**) 0.61/0.61/5.4/0.152; (**f**) 0.61/0.31/1.5/0.152; (**g**) 0.61/0.15/1.35/0.152. The slopes of the straight lines yield the pseudo-first-order rate constants k_{Th}^1 for TEOS hydrolysis

As can be seen from Fig. 2, the exponentially fitted time-dependent concentration of Q_0^0 is a good approximation to the experimental data. In this case, it is assumed that the reaction (7) is of first order, *i.e.*, $\alpha = 1$, so the rate expression (17) reduces to:

$$r_{\mathrm{T}} = -\frac{\mathrm{d}\left[Q_0^0\right]}{\mathrm{d}t} = k_{\mathrm{Th}}^1\left[Q_0^0\right] \tag{18}$$

Integration of Eq. (18) then yields

$$\ln\left[Q_0^0\right] = \ln\left[Q_0^0\right]_0 - k_{\mathrm{Th}}^1 t \tag{19}$$

Thus, a plot of $\ln[Q_0^0]$ *versus* t should yield a straight line with $-k_{\mathrm{Th}}^1$ as the slope and $\ln[Q_0^0]_0$ as the intercept. Figure 3 shows the relation between $\ln[Q_0^0]$ and t. The observed good linearity proves that $\alpha = 1$. Furthermore, taking the natural logarithm of Eq. (16) yields,

$$\ln k_{\mathrm{Th}}^1 = \ln k_{\mathrm{Th1}} + \beta \ln[\mathrm{NH_3}] + \gamma \ln[\mathrm{H_2O}]. \tag{20}$$

Therefore, a linear plot of $\ln\, k_{\mathrm{Th}}^1$ *versus* $\ln[\mathrm{NH_3}]$ with a slope β will yield the reaction order β for NH_3 when $[H_2O]$ is assumed to remain constant (*i.e.*, samples (a), (b) and (c)). This plot is shown in Fig. 4. Similarly, a linear plot of $\ln\, k_{\mathrm{Th}}^1$ *versus* $\ln[\mathrm{H_2O}]$, shown in Fig. 5, will yield the reaction order γ of H_2O when $[NH_3]$ remains constant (*i.e.*, samples (a), (d), (e)). Values of $\beta = 0.98$ and $\gamma = 0.795$ have been determined directly from the TEOS branches of Figs. 4 and 5. The relative deviations for β and γ are less than 5%, and originated from uncertainties in the area integration of the NMR peaks. Applying the value of k_{Th}^1 obtained from Fig. 3, and using values of β and γ in Eq. (20), the values of k_{Th1} were calculated (see Table 3). Finally, the initial hydrolysis rate equation for TEOS in the mixed TEOS/DDS system is

$$r_{\mathrm{T}} = 9.33 \times 10^{-3}[\mathrm{TEOS}][\mathrm{NH_3}]^{0.98}[\mathrm{H_2O}]^{0.795} \tag{21}$$

From Eqs. (7) and (9), the disappearance of species Q_0^1 is accompanied by the appearance of the condensation product species Q_1^0, or a cross-condensed species and another intermediate species Q_0^3. Because the intermediate Q_0^1 is so active that it has little time to accumulate, a steady-sate concentration is reached after the Q_0^1 concentration approaches its maximum

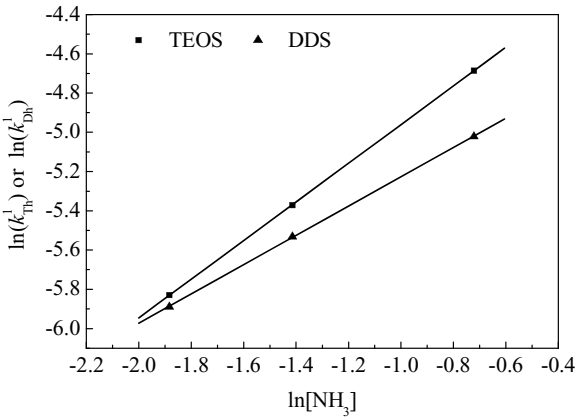

Fig. 4 Pseudo-first-order hydrolysis rate constants k^1_{Th} and k^1_{Dh} *versus* the NH_3 concentration in the TEOS/DDS systems (the linear correlation coefficients are 0.99996 and 0.99999 for TEOS and DDS, respectively)

value. According to the steady-state approximation [39], the following equation is obtained:

$$\frac{d[Q_0^1]}{dt} = k_{Th1}[Q_0^0]_{ss} - k_{Tc1}[Q_0^1]_{ss} \approx 0 \tag{22}$$

where $[Q_0^1]_{ss}$ and $[Q_0^0]_{ss}$ are the steady-state concentrations of $[Q_0^1]$ and $[Q_0^0]$, respectively. Hence, the condensation rate constant k_{Tc1} can be defined by:

$$k_{Tc1} = k_{Th1}\frac{[Q_0^0]_{ss}}{[Q_0^1]_{ss}} \tag{23}$$

The k_{Tc1} data are also listed in Table 3. Because Q_0^3 does not appear in experiments (f) and (g), k_{Th2} and k_{Tc2} that are defined by reactions (5) and (7) are not taken into account.

3.2.3 Hydrolysis kinetics of DDS in TEOS/DDS mixtures

Applying an analysis process similar to that used for TEOS for calculating the hydrolysis kinetics of DDS in the mixed TEOS/DDS system, reaction (11), three plots of $\ln[D_0^0]$ *versus*

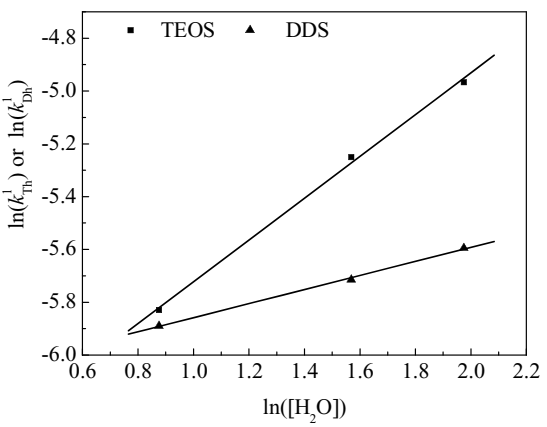

Fig. 5 Pseudo-first-order hydrolysis rate constants k^1_{Th} and k^1_{Dh} *versus* the H_2O concentration in the TEOS/DDS systems (the linear correlation coefficients are 0.999905, and 0.99992 for TEOS and DDS, respectively)

Table 3 Rate constants for hydrolysis and condensation in the TEOS/DDS systems

Sample	$^{a}k_{Th1} \times 10^3$ (TEOS)	$^{a}k_{Dh1} \times 10^3$ (DDS)	$^{a}k_{Tc1} \times 10^3$ (TEOS)	$^{a}k_{Dc1} \times 10^3$ (DDS)
(a)	10.64 ± 0.5	9.39 ± 0.45	61.29 ± 3.2	63.69 ± 3.2
(b)	9.42 ± 0.5	9.09 ± 0.45	69.04 ± 3.5	54.08 ± 2.7
(c)	8.72 ± 0.44	8.83 ± 0.42	63.76 ± 2.2	51.65 ± 2.6
(d)	9.68 ± 0.48	9.02 ± 0.45	65.47 ± 3.3	53.1 ± 2.7
(e)	9.53 ± 0.48	9.54 ± 0.48	67.69 ± 3.4	60.47 ± 3.1
(f)	9.67 ± 0.48	8.77 ± 0.44	67.95 ± 3.4	57.88 ± 2.9
(g)	9.06 ± 0.45	9.50 ± 0.48	70.01 ± 3.5	56.12 ± 2.8
Average	9.33 ± 0.47	9.16 ± 0.48	66.5 ± 0.5	56.7 ± 0.48
^{b}Reference	7.41 ± 0.4	28.14 ± 1.4	157.2 ± 0.4	35.19 ± 1.8

[a] The errors of k_h and k_c were estimated assuming a 5% uncertainty for the integration areas, and subscripts h and c indicate hydrolysis and condensation reactions, respectively.
[b] Reference experiments refer to the individual hydrolysis of single precursor species under the same reactive conditions as used in this paper.

t, $\ln k^1_{Dh}$ *versus* $\ln[NH_3]$, and $\ln k^1_{Dh}$ *versus* $\ln[H_2O]$ have been drawn and are shown in Fig. 6; the DDS branch of Fig. 4 and the DDS branch of Fig. 5, respectively. Consequently, the hydrolysis rate equation for DDS was obtained as:

$$r_D = 9.16 \times 10^{-3}[DDS][NH_3]^{0.75}[H_2O]^{0.26} \tag{24}$$

Using the steady-state approximation [39], the condensation rate constant k_{Dc1} has also been defined and its values are listed in Table 3.

3.3 Results of ^{29}Si MAS NMR and XPS measurements on xerogels

Figure 7a and b shows the solid-state ^{29}Si MAS NMR spectra of the hybrid gels (a) and (g), respectively, where the superscripts m and n in the symbols Q^m and D^n denote the number of Si−O−Si bridges. As to gel (a), mainly the D^2 peak of DDS condensation and the Q^4 peak of TEOS condensation are simultaneously observed. As for gel (g), the strong Q^4 signal reveals the high extent of condensation of TEOS, but DDS has a very low condensation

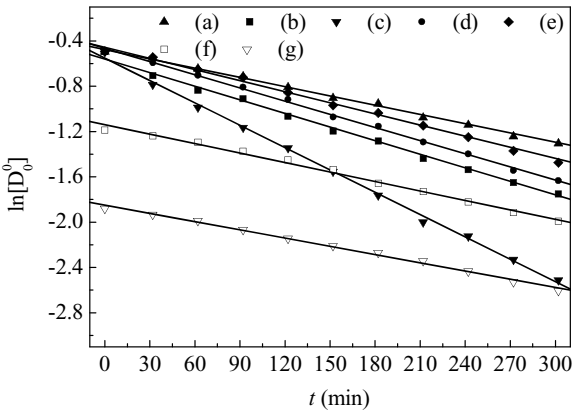

Fig. 6 Time-dependent DDS monomer concentrations in the TEOS/DDS systems with the molar ratio of TEOS/DDS/H_2O/NH_3 at: (**a**) 0.61/0.61/1.8/0.152; (**b**) 0.61/0.61/1.8/0.243; (**c**) 0.61/0.61/1.8/0.486; (**d**) 0.61/0.61/3.6/0.152; (**e**) 0.61/0.61/5.4/0.152; (**f**) 0.61/0.31/1.5/0.152; (**g**) 0.61/0.15/1.35/0.152. The slopes of the straight lines yield the pseudo-first-order rate constants k^1_{Dh} for DDS hydrolysis

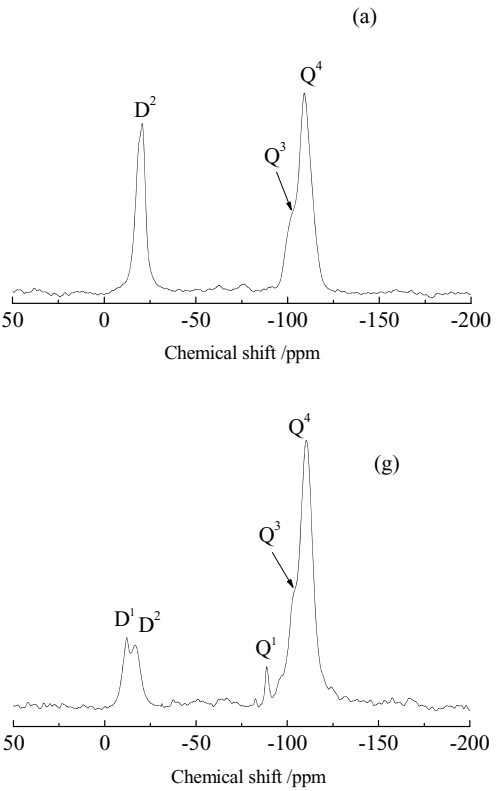

Fig. 7 Solid-state ^{29}Si MAS NMR spectra of TEOS/DDS hybrid gels (**a**) and (**g**)

extent because both D resonance signals appear, including D^1 (for partial condensation) and D^2 (for complete condensation).

The atomic content (AC) of carbon on the hybrid SiO_2 particle surface was calculated from the integral area of the carbon peak of the XPS spectrum. For hybrid gel (a), the AC is as high as 50.45%, which means there was enrichment of methyl groups on the surface of the SiO_2 particles. The error of the AC value originated from the relative uncertainty of about 5% of the integral area.

3.4 Results of SAXS and TEM

The SAXS technique has been successfully applied to the characterization of nano-scale microstructures [40–43], especially the fractal structure of sols, although it cannot provide chemical kinetic information for a sol. The SAXS of a typical fractal system has an exponential decrease of the scattering intensity that is given by $I(q) \alpha q^{-\mathrm{Dm}} (1 \leq \mathrm{Dm} < 3)$ or $I(q) \alpha q^{\mathrm{Ds}-6}$ $(2 < \mathrm{Ds} < 3)$ for mass-fractal systems (the fractal dimension is Dm) or surface-fractal systems (the fractal dimension is Ds), respectively [45], where $q = (4\pi/\lambda \sin(\theta/2))$ is the scattering wave vector, λ is the wavelength of the incident X-ray and θ is the scattering angle. Thus, a fractal curve of $\ln[I(q)]$ *versus* $\ln(q)$ will possess a linear range with $-\mathrm{Dm}$ as its slope. The fractal dimension can be determined from the slope of the linear range. According to Craievich [45] and Marliere *et al.* [46], it is possible for double-fractal structures to exist. That is, a complex fractal structure is present that includes two fractal dimensions.

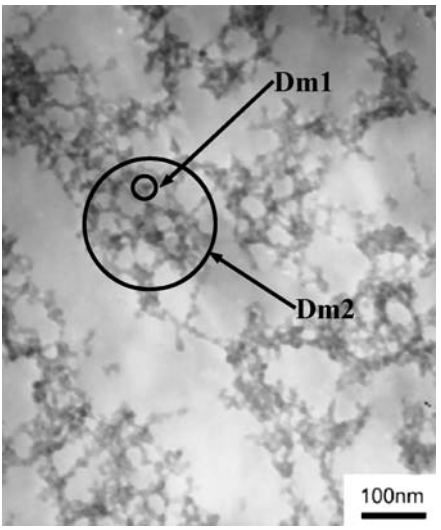

Fig. 8 TEM photographs of TEOS/DDS hybrid sol

The detailed fractal data are collected in Table 5 from which two fractal dimensions can be found for the TEOS/DDS hybrid sols. Both Dm1 and Dm2 are mass-fractals and $2 < Dm1 < 3$, $1 < Dm2 < 2$. This double-fractal structure can be confirmed from the TEM photograph shown in Fig. 8. In Fig. 8, two circles indicate the spacial scale of the double-fractal structure, of which the small one is for primary particles (corresponding to Dm1) and the large one for particulate networks (corresponding to Dm2). Obviously, the primary particles are linked together into some loose networks.

4 Discussion

4.1 Comparison with the hydrolysis and condensation of a single precursor

The main reason for studying the hydrolysis and condensation of the TEOS/DDS mixed systems is to understand the hybrid sol-gel process at a molecular level along with the subsequent microstructure and chemical homogeneity of the derived hybrid materials. A clear analysis of the hydrolysis kinetics will provide us with effective directions to synthesize hybrid materials in the light of special material design requirements. Thus, the first thing to be dealt with is identifying both why and what kind of differences occur between the hydrolysis kinetics of the mixed double-precursor system and those of the single precursor systems.

According to our previous work [31], the individual hydrolysis rate equations for the single TEOS and DDS systems are of the following type:

$$r_T = 7.41 \times 10^{-3}[\mathrm{TEOS}][\mathrm{NH_3}]^{0.333}[\mathrm{H_2O}]^{0.227} \tag{25}$$

$$r_\mathrm{D} = 2.814 \times 10^{-2}[\mathrm{DDS}][\mathrm{NH_3}]^{0.652}[\mathrm{H_2O}]^{0.080} \tag{26}$$

Comparing Eq. (18) with (22), and Eq. (21) with (23), it is obvious that the reaction orders of NH_3 and H_2O become larger in the mixed double-precursor system than in the single-precursor system. This result indicates that the hydrolysis of TEOS and the hydrolysis of

DDS are more sensitive to the concentrations of NH_3 and H_2O in the mixed-precursor system than in the single-precursor system. In addition, the reactive order with respect to the NH_3 concentration is always larger than that of H_2O, which shows a stronger sensitivity of the hydrolysis to the concentration of NH_3 than to H_2O. These results reveal an important phenomenon: TEOS and DDS both follow their original reaction pathways even in mixed systems and the sequence of sensitivity is still in the order TEOS (DDS) > NH_3 > H_2O. Thus, one need not worry about a possible irregular change in the sensitivity sequence. This conclusion is useful for the design of hybrid materials.

In the reference experiments for the single-precursor systems, the hydrolysis rate constants k_{Th1} for TEOS and k_{Dh1} for DDS are listed in the row "reference" of Table 3. It was found that k_{Th1} increases from 7.41×10^{-3} to 9.33×10^{-3} when the situation for TEOS is changed from the single-precursor system to the mixed-precursor system. On the contrary, k_{Dh1} decreases from 28.14×10^{-3} to 9.16×10^{-3} when the situation of DDS is changed from the single to the mixed-precursor system. However, the value of k_{Tc1} decreases from 157.2×10^{-3} to 66.5×10^{-3} and the value of k_{Dc1} increases from 35.19×10^{-3} to 56.7×10^{-3}. If we define the following two variables $K_{\mathrm{T}} = k_{\mathrm{Tc1}}/k_{\mathrm{Th1}}$ for TEOS and $K_{\mathrm{D}} = k_{\mathrm{Dc1}}/k_{\mathrm{Dh1}}$ for DDS, the relative rates between the condensation and hydrolysis reactions can be seen more clearly. The obtained values of K_{T} and K_{D} are collected in Table 4. Interestingly, the divergence between the values of K_{T} and K_{D} decreases from 21.2 to 1.2 and from 7.5 to 6.1, respectively, when the TEOS and DDS situations are changed from the single-precursor system to the mixed-precursor system, which shows that a more compatible sol-gel process occurs between TEOS and DDS. This information should benefit the fabrication of hybrid materials with higher homogeneity.

Comparing the condensation rates for systems (g), (f), (a) in Table 3, some useful information can be obtained. With the increasing concentration of DDS in the mixed-precursor systems, the condensation rate of TEOS decreases whereas the condensation rate of DDS increases. This can be understood from the reduction of the average functionality for silicon atoms of TEOS a phenomenon that prevents formation of the siloxane network. The reverse case occurs for DDS.

In summary, hydrolysis becomes more active and the reactive behavior of TEOS and DDS becomes more compatible in the TEOS/DDS mixed-precursor system, compared with the corresponding single-precursor systems. All these phenomena indicate the possibility of forming a product with high homogeneity.

4.2 Estimation of cross condensation and particle growth

Although the hydrolysis kinetics and the simple condensation rate constants of the mixed TEOS/DDS systems have been determined, the condensation kinetics, especially the cross-condensation kinetics, are impossible to study using the liquid-state NMR technique under

Table 4 Relative rates for hydrolysis and condensation[a]

	K_{T} (TEOS)	K_{D} (DDS)
Mixed precursor system	7.5	6.1
Single precursor system	21.2	1.2

[a] $K_T = k_{\mathrm{Tc1}}/k_{\mathrm{Th1}}$ and $K_{\mathrm{D}} = k_{\mathrm{Dc1}}/k_{\mathrm{Dh1}}$, where k_{Tc1} and k_{Th1} are the condensation and hydrolysis rate constants for TEOS, and k_{Dc1} and k_{Dh1} are the condensation and hydrolysis rate constants for DDS.

basic condition. This is because the condensation reaction occurs faster than the hydrolysis reaction and the formed condensation species immediately participate in nucleation and become inaccessible to liquid-state NMR measurements. The defined condensation rate constants k_{Tc} and k_{Dc} are just overall rate constants for TEOS and DDS, and no cross-condensation reaction kinetics were described. After gelation occurs, the solid-state ^{29}Si NMR method is suitable for analyzing the local chemical environment in the hybrid materials. But, no appropriate technique is available to study the condensation kinetics and growth kinetics of particles that occur just in the "blind" region between the liquid-state NMR detection range and the solid-state NMR detection range.

However, we can still approximately understand the cross-condensation properties using the solid-state ^{29}Si MAS NMR and XPS methods. Figure 7 shows the solid-state ^{29}Si MAS NMR spectra of the hybrid gels resulted from samples (a) and (g). As to sample (a), the strong Q^4 and D^2 signals reveal a high extent of condensation of TEOS and DDS. However, for sample (g), the DDS precursor shows a very low extent of condensation because all of the D resonance signals from D^1 (partial condensation) to D^2 (complete condensation) coexist. This contradictory situation should not occur when cross condensation between the hydrolyzed TEOS and DDS is intense. The XPS result shows that the concentration of carbon on the surface of the hybrid-gel particle is 50.45%. Thus, the methyl groups introduced by the DDS-TEOS cross condensation are mainly distributed on the surface of the hybrid gel. Combining the results from the solid-state ^{29}Si MAS NMR and XPS measurements, we deduce that cross condensation is weak for the hybrid sol-gel process under basic conditions. But, from the hydrolysis kinetics measurements, the hydrolysis and condensation rates of TEOS and DDS are more compatible. In spite of this extent of cross condensation, it is closely related to the particle growth.

It is difficult for the actual growth mechanism of particles to be completely characterized because of the complex effects from the solvent and reaction compositions. Only for the simplest system TEOS/EtOH/H_2O/NH_3 is the growth mechanism of SiO_2 particles considered to be clear. That is, a standard reaction-limited growth occurs with no formation of new particles and no agglomeration of existing particles [27]. In addition, the effect of the solvent on the particle growth is an important aspect. Mine and co-workers [28] investigated the effect of different alcohol solvents on the particle growth rate and found that differences in the dielectric constant of the solvent and the particle surface potential determined the magnitudes of the inter-particle repulsion and the corresponding order of the particle growth rate. Concerning our binary precursor systems, the mechanism of particle growth should be more complex than for the single precursor system. The true situation may be the following: TEOS hydrolyzes and self-condenses into some silica nuclei; simultaneously, the hydrolyzed DDS reacts with these nuclei and modifies the surface of the silica particles with methyl groups that then prevents particle agglomeration and adds to the insolubility of the colloidal silica particles.

4.3 Double fractal structure in TEOS/DDS hybrid sol

There is still the question as to how the double-fractal structures come into being in the hybrid sols, even though the reaction kinetics and the cross condensation have been studied. To answer this question, the relative hydrolysis rate between DDS and TEOS, r_T/r_D, is the key. In the above-mentioned discussion about K_T and K_D, a better compatibility between the hydrolysis and condensation of TEOS or DDS was found. It accounts qualitatively for the easier hybrid formation between TEOS and DDS. The ratio r_T/r_D can be used to explain how the starting condition of the hybrid sol affects the double-fractal structure. The values

Table 5 Values of r_T/r_D and the detailed double-fractal structure parameters[a]

Sample	r_T/r_D	Dm1	Dm2
(a)	1.05	2.31	1.26
(b)	1.17	2.22	1.11
(d)	1.52	2.29	1.21
(g)	3.27	2.26	1.07

[a] Dm1 and Dm2 are the mass-fractal dimensions; $r_T/r_D = 1.02[\mathrm{TEOS}][\mathrm{NH_3}]^{0.23}[\mathrm{H_2O}]^{0.53}/[\mathrm{DDS}]$.

of r_T/r_D (its relative deviations are less than 5%, which originates from uncertainties in the area integration of the NMR peaks) are calculated from Eqs. (21) and (24) as follows:

$$r_T/r_D = \frac{9.33 \times 10^{-3}[\mathrm{TEOS}][\mathrm{NH_3}]^{0.98}[\mathrm{H_2O}]^{0.795}}{9.16 \times 10^{-3}[\mathrm{DDS}][\mathrm{NH_3}]^{0.75}[\mathrm{H_2O}]^{0.26}} = 1.02[\mathrm{TEOS}][\mathrm{NH_3}]^{0.23}[\mathrm{H_2O}]^{0.535}/[\mathrm{DDS}] \quad (27)$$

The detailed r_T/r_D values are collected in Table 5. Comparing samples (a) with (b), (a) with (d), and (a) with (g), respectively, it is found that the r_T/r_D values increase with $[\mathrm{NH_3}]$, $[\mathrm{H_2O}]$ and the ratio of TEOS to DDS. Simultaneously, the amounts of Dm2 increase against this sequence.

TEOS hydrolyzes and self-condenses into the compact silica nuclei with Dm1 being greater than two. The simultaneously hydrolyzed DDS monomers cross condense with the Si−OH groups on the surface of the compact silica nuclei and further link them into a loose network with Dm2 being smaller than two. In this process, the relative hydrolysis rates between TEOS and DDS determine how loose the particulate network will be. For example, the value of r_T/r_D of sample (a) is 1.05 and is much smaller than 3.27 of sample (g), which mean that a smaller difference between the hydrolysis rates occurs between TEOS and DDS for sample (a) than for (g). Thus, the hydrolyzed DDS will quickly cross condense with the hydrolyzed TEOS to block further growth of SiO_2 particles. This growth prevention is remarkable so that DDS has a good condensation rate (see the ^{29}Si MAS NMR result of Fig. 7a).

Taking the particle size into account, the sol (a) undergoes faster particulate growth than sol (g). Therefore, TEOS and DDS must hybridize into a somewhat more compact network in sol (a) than in sol (g). This can be verified by their fractal dimension Dm2, as seen in Table 5. Although the particulate networks of sol (a) and sol (g) all possess typical double-fractal structures, the Dm2 of sol (a) is larger than that of sol (g). Based upon the comparative analysis between r_T/r_D and Dm2 of the hybrid sols (a) and (g), these two parameters are only different aspects of the same nature. Thus it is reasonable to find such concordant results by different methods.

5 Conclusion

Because the condensation of siloxane is much faster than its hydrolysis under basic conditions, and the species formed by condensation participate by nucleation immediately and become insoluble, it is difficult to detect the liquid-state ^{29}Si NMR signal of the condensed species. Therefore, only the kinetics of the initial hydrolysis of the TEOS/DDS mixed systems have been observed. The most valuable conclusion is that the hydrolysis and condensation of TEOS and DDS become more compatible in the double-precursor system than in single-precursor system. Assisted by information gained from the solid ^{29}Si MAS, NMR and XPS

measurements, weak cross condensation between two precursors can be deduced. The true hybrid sol-gel process may be the following: TEOS hydrolyzes and self-condenses into silica nuclei, simultaneously the hydrolyzed DDS modifies the surface of the silica nuclei and results in double-fractal clusters through cross condensation with the silica nuclei. Thus, *in-situ* liquid-state ^{29}Si NMR provides a powerful tool for studying the initial hydrolysis kinetics, which is crucial for formation of the structure and homogeneity of the final hybrid material. Although no appropriate experimental technique could be utilized to obtain directly the condensation kinetics, the cross-condensation mechanism can still be estimated with the assistance of solid ^{29}Si MAS NMR and XPS and SAXS measurements. This supplements the kinetics studies.

Acknowledgments Financial support from the National Key Native Science Foundation (No. 20133040) is gratefully acknowledged.

References

1. Brinker, C.J., Scherer, O.W.: Sol-gel Science: the Physics and Chemistry of Sol-gel Processing. Academic Press, San Diego (1990)
2. Hench, L.L., West, J.K.: The sol-gel process. Chem. Rev. **90**, 33–72 (1990)
3. Cheetham, A.K., Brinker, C.J., Mecartney, M.L., Sanchez, C. (eds.): Better ceramics through chemistry V. Materials Research Society, Pittsburgh (1994)
4. Mackenzie, J.D., Bescher, E.P.: Structure, properties and potential application of ormosils. J. Sol-Gel Sci. Tech. **13**, 371–377 (1998)
5. Mackenzie, J.D.: Sol-gel research – achievements since 1981 and prospects for the future. J. Sol-Gel Sci. Tech. **26**, 23–27 (2003)
6. Innocenzi, P., Brusotin, G., Guglielmi, M., Bertani, R.: New synthetic route to (3-glycidoxypropyl)triethoxysilane-based hybrid organic-inorganic materials. Chem. Mater. **11**, 1672–1679 (1999)
7. Schottner, G.: Hybrid sol-gel-derived polymers: applications of multifunctional materials. Chem. Mater. **13**, 3422–3435 (2001)
8. Zhang, Y., Wang, M.Q.: Mechanical characterization and optical properties analysis of organically modified silicates. J. Non-Cryst. Solids **271**, 88–93 (2000)
9. Liu, Y., Ren, W., Zhang, L.Y., Yao, X.: New method for making porous SiO_2 thin films. Thin Solid Films **353**, 124–128 (1999)
10. Kuraoka, K., Kubo, N., Yazawa, T.: Microporous silica xerogel membrane with high selectivity and high permanence for carbon dioxide separation. J. Sol-Gel Sci. Tech. **19**, 515–518 (2000)
11. Green, D.L., Lam, S., Jayasundara, Y.F., Harris, M.T.: Chemical reaction kinetics leading to the first Stober silica nanoparticles-NMR and SAXS investigation. J. Non-Cryst. Solids **315**, 166–179 (2003)
12. Blaaderen, A.V., Vru, A.: Synthesis and characterization of monodisperse colloidal organo-silica spheres. J. Colloid Interfac. Sci. **156**, 1–18 (1993)
13. Assink, R.A., Kay, B.D.: Sol-gel kinetics I. Functional group kinetics. J. Non-Cryst. Solids **99**, 359–370 (1988)
14. Kay, B.D., Assink, R.A.: Sol-gel kinetics: II. Chemical speciation modeling. J. Non-Cryst. Solids **104**, 112–122 (1988)
15. Sadasivan, S., Dubey, A.K., Li, Y.Z., Rasamussen, D.H.: Alcoholic solvent effect on silica synthesis – NMR and DLS investigation. J. Sol-Gel Sci. Tech. **12**, 5–14 (1998)
16. Bogush, G.H., Zukoski, C.F.: Studies of the kinetics of the precipitation of uniform silica particles through the hydrolysis and condensation of silicon alkoxides. J. Colloid. Interfac. Sci. **142**, 1–18 (1991)
17. Fyfe, C.A., Zhang, Y., Aroca, P.: An alternative preparation of organofunctionalized silica gel and their characterization by two-dimensional high-resolution solid-state heteronuclear NMR correlation spectroscopy. J. Am. Chem. Soc. **114**, 3252–3255 (1992)
18. Hook, R.J.: A ^{29}Si NMR study of the sol-gel polymerization rates of substituted ethoxysilanes. J. Non-Cryst. Solids **195**, 1–15 (1996)
19. Riegel, B., Blittersdorf, S., Kiefer, W., Hofacker, S., Schottner, G.: Kinetic investigations of hydrolysis and condensation of the glycidoxypropyltrimethoxy silane/aminopropyltriethoxy-silane system by means of FT-Raman spectroscopy I. J. Non-Cryst. Solids **226**, 76–84 (1998)

20. Riegel, B., Blittersdorf, S., Kiefer, W., Husing, N., Schubert, U.: Raman spectroscopic analysis of the sol-gel processing of $Rsi(OMe)_3/Si(Ome)_4$ mixtures. J. Molec. Struct. **410/411**, 157–160 (1997)
21. Prabakar, S., Assink, R.A.: Hydrolysis and condensation kinetics of two component organically modified silica sols. J. Non-Cryst. Solids **211**, 39–48 (1997)
22. Prabakar, S., Assink, R.A., Raman, N.K., Myers, S.A., Brinker, C.J.: Identification of self- and cross-condensation products in organically modified silica sols by ^{29}Si and ^{17}O NMR spectroscopy. J. Non-Cryst. Solids **202**, 53–60 (1996)
23. Alie, C., Pirard, J.P.: Preparation of low-density xerogels from mixtures of TEOS with substituted alkoxysilanes. I. ^{17}O NMR study of the hydrolysis-condensation process. J. Non-Cryst. Solids **320**, 21–30 (2003)
24. Brus, J., Dybal, J.: Copolymerization of tetraethoxysilane and dimethyl(diethoxy) silane studied by ^{29}Si NMR and ab initio calculations of ^{29}Si NMR chemical shifts. Polymer, **40** (1999) 6933–6945
25. Brus, J.: Solid-state NMR study of phase separation and order of water molecules and silanol groups in polysiloxane networks. J. Sol-Gel Sci. Tech. **25**, 17–28 (2002)
26. Wonorahardjo, S., Ball, G.E., Hook, J., Moran, G.: ^{2}H NMR relaxation monitoring of gelation in tetramethoxysilane sol-gels. J. Non-Cryst. Solids **271**, 137–146 (2000)
27. Satoh, T., Akitaya, M., Konno, M, Saito, S.: Particle size distributions produced by hydrolysis and condensation of tetraethylorthosilicate. J. Chem. Eng. Japan **30**(4), 759–762 (1997)
28. Mine, E., Nagao, D., Kobayashi, Y., Konno, M.: Solvent effects on particle formation in hydrolysis of tetraethyl orthosilicate. J. Sol-Gel Sci. Tech. **35**(3), 197–201 (2005)
29. Brus, J., Spirkova, M., Hlavata, D., Strachota, A.: Self-organization, structure, dynamic properties, and surface morphology of silica/epoxy films as seen by solid-state NMR, SAXS, and AFM. Macromolecules **37**(4), 1346–1357 (2004)
30. Brinker, C.J.: Hydrolysis and condensation of silicates: Effects on structure. J. Non-Cryst. Solids **100**, 31–50 (1988)
31. Liu, R., Xu, Y., Wu, D., Sun, Y., Gao, H., Yuan, H., Deng, F.: Comparative study on the hydrolysis kinetics of substituted ethoxysilanes by liquid-state ^{29}Si NMR. J. Non-Cryst. Solids **343**, 61–70 (2004)
32. Iler, R.K.: The Chemistry of Silica. Wiley, New York (1979)
33. Keefer, K.D.: In: C.J. Brinker, D.E. Clark, D.R. Ulrich (eds.) Better ceramics through chemistry, p. 15. North-Holland, New York (1984)
34. Pohl, E.R., Osterholtz, F.D.: In: Ishida, H., Kumar, G. (eds.) Molecular Characterization of Composite Interfaces, p. 157. Plenum, New York (1985)
35. Voronkov, M.G., Mileshkevich, V.P., Yuzhelevski, Y.A.: The Siloxane Bond. Consultants Bureau, New York (1978)
36. Assink, R.A., Kay, B.D.: Sol-gel kinetics III. Test of the statistical reaction model. J. Non-Cryst. Solids **107**, 35–40 (1988)
37. Assink, R.A., Kay, B.D.: In: Brinker, C.J., Clark, D.E., Ulrich, D.R. (eds.) Better Ceramics through Chemistry, p. 301. North-Holland, New York (1984)
38. Lee, K., Look, J.L., Harris, M.T., McCormick, A.V.: Assessing extreme models of the Stöber synthesis using transients under a range of initial composition. J. Colloid. Interfac. Sci. **194**, 78–88 (1997)
39. Xu, Y., Liu, R., Wu, D., Sun, Y., Gao, H., Yuan, H., Deng, F.: Ammonia-catalyzed hydrolysis kinetics of mixture of tetraethoxysilane with methyltriethoxysilane by ^{29}Si NMR. J. Non-Cryst. Solids **351**, 2403–2413 (2005)
40. Boukari, H., Lin, J.S., Harris, M.T.: Probing the dynamics of the silica nanostructure formation and growth by SAXS. Chem. Mater. **9**, 2376–2384 (1997)
41. Boukari, H., Long, G., Harris, M.T.: Polydispersity during the formation and growth of the Stober silica particles from small angle X-ray scattering measurements. J. Colloid. Interf. Sci. **229**, 129–139 (2000)
42. Berthon, S., Barbieri, O., Ehrburger-Dolle, F.: DLS and SAXS investigations of organic gels and aerogels. J. Non-Cryst. Solids **285**, 154–161 (2001)
43. Krakovsky, I., Urakawa, H., Kajiwara, K., Kohjiya, S.: Time resolved small angle X-ray scattering of inorganic-organic gel formation kinetics. J. Non-Cryst. Solids **231**, 31–40 (1998)
44. Keefer, K.D., Schaefer, D.W.: Growth of fractal rough colloids. Phys. Rev. Lett. **56**, 2376–2379 (1986)
45. Craievich, A.F.: SAXS study of the porous fractal structure of tricalcuim silicate dry gels. J. Appl. Crystallogr. **20**, 327–329 (1987)
46. Marliere, C., Despetis, F., Etienne, P., Phalippou, J.: Two fractal structures in aerogel. J. Non-Cryst. Solids **285**, 175–180 (2001)